AIAA JOURNAL
Vol. 47, No. 4, April 2009

Multichannel Spectral and Coherence Analysis of Servoflap Main Rotor Blade

Taikang Ning*
Trinity College, Hartford, Connecticut 06106
and
Fu-Shang (John) Wei†
Kaman Aerospace Corporation, Bloomfield, Connecticut 06002

DOI: 10.2514/1.38485

Flight performance of servoflap rotor helicopters is linked closely with the relationship between the servoflap and the rotor blade; rotor performance can be improved and fuselage vibration can be reduced when the feedback control for a servoflap is properly configured at multiple harmonics of the rotating (1/rev) frequency. In this paper, we have examined helicopter servoflap and main rotor blade parameters via multichannel spectral and coherence analysis. In particular, we have examined servoflap bending, rotor blade flatwise bending at 17 and 24% of the blade radius, and blade torsion at 38% of the blade radius using helicopter vibratory data collected during four representative flight conditions: hover, transition, minimum-power and cruising-speed forward flights. The analysis includes two steps: 1) identifying vibratory energy concentrations of servoflap bending and rotor blade flatwise bending and torsion at multiple harmonics of 1/rev frequency, and 2) quantifying the linear relationships of these spectral energy concentrations between servoflap bending and rotor blade flatwise bending and torsion with measures of magnitude squared coherence function and phase (time) delay. Using these quantitative descriptors, we analyzed helicopter vibratory data during four different flight conditions, summarized spectral energies of the first eight harmonics of 1/rev frequency, and delineated the linear relationships between the servoflap and rotating system parameters. The multichannel spectral and coherence analysis results have generated useful baseline data to assist continual improvement in servoflap rotor design.

Nomenclature

$Adv17$	=	minimum-power forward flight
$Adv27$	=	cruising-speed forward flight
$B17f$	=	rotor blade flatwise bending at 17% of the blade radius
$B24f$	=	rotor blade flatwise bending at 24% of the blade radius
$B38t$	=	rotor blade torsion at 38% of the blade radius
C_L	=	lift coefficient
C_{L0}	=	blade lift at zero angle of attack
$C_{L\alpha}$	=	blade lift curve slope
$C_{L\delta}$	=	servoflap lift curve slope
C_d	=	drag coefficient
$\mathrm{coh}_{i,j}(f)$	=	coherence function
dL	=	blade element lift
dQ	=	blade element torque
$Engy\_dc$	=	vibratory energy index related to static deformation
$Engy\_vbr$	=	vibratory energy index related to dynamic deformation
$Flap$	=	servoflap vertical bending
f	=	frequency
$Hover$	=	hover flight
$K_{\delta\beta}$	=	flapping to servoflap feedback coupling coefficient
$K_{\delta\theta}$,	=	feathering to servoflap feedback coupling coefficient
$K_{\delta\zeta}$	=	lag to servoflap feedback coupling coefficient
r	=	rotor blade radius
$S_{i,i}(f)$	=	autospectrum
$S_{i,j}(f)$	=	cross spectrum
$Trans$	=	transition flight
v'	=	in-plane bending slope
w'	=	out-of-plane bending slope
$X_i^k(f)$	=	Fourier transform of the kth data segment of channel i
α	=	rotor blade angle of attack
δ	=	servoflap angle
δ_{input}	=	servoflap input control
δ_0	=	collective control input
δ_{1s}, δ_{1c}	=	cyclic control input
θ	=	blade feathering displacement—leading edge up from the shaft plane, deg
μ_k	=	mean value of kth data segment
$\Phi(f)$	=	multichannel spectral density matrix
ϕ	=	inflow angle
ψ	=	blade azimuth position, deg
1/rev	=	rotating speed of rotor blade
$*$	=	complex conjugate

I. Introduction

SINCE its inception more than half a century ago, the helicopter industry [1,2] has witnessed continual technical advancement in many areas, such as rotor blade design, rotorcraft aerodynamics, computer based design and simulation tools, and modern avionics, to name a few. To a large extent, among all recently developed technical innovations, newer and better rotor blade designs undoubtedly have contributed most to improve the overall performance efficiency for helicopter flight. To date, many creative rotor blade system designs have emerged with enhanced and satisfactory performance; one particular design approach for rotor-based aircrafts that has captured the attention of the industry is to shift the conventional pitch-horn rotor blade control from the fixed system to the rotating system through servoflaps [3,4]. A servoflap (Fig. 1) is a small airfoil section placed on the trailing edge of the blade that operates under high

Received 10 May 2008; revision received 9 December 2008; accepted for publication 23 December 2008.

*Associate Professor and Chair, Department of Engineering. Member AIAA.
†Chief Engineer, Aeromechanics. Member AIAA.

Fig. 1 A production composite rotor blade with an external servoflap.

Fig. 2 Cross-section view of an external servoflap rotor blade.

rotational speed and centrifugal force conditions, normally around $530g$ depending on the nominal rotor rpm. The cross-section view of an external servoflap rotor is shown in Fig. 2. This unorthodox design concept eliminates the need for a hydraulic boost control system and replaces it with a much smaller, lighter, and simpler mechanism (servoflap) that requires moderate control forces [3–7] to turn large, heavy rotor blades to the desired angle of attack in various flight conditions. Such a design translates into significant helicopter control system weight reduction and renders a servoflap rotor the best viable candidate for an unmanned, aerial vehicle [5,8] in the future.

In general, a servoflap rotor is a very stable system for generating blade thrust and pitching moment. For example, when the servoflap produces an upload on the flap, it leads to a nose-down pitching moment with respect to the main rotor feathering axis to decrease the blade angle of attack. When the servoflap produces a download on the flap, it produces a nose-up pitching moment with respect to the main rotor feathering axis. By way of up- or downloads, the servoflap can be used to meet the required rotor thrust and blade angle of attack at varying flight conditions. The servoflap adds an extra degree of freedom to rotor behavior and gives rise to a rotor system design that is both interesting and challenging; a servoflap based rotor blade exhibits some essentially different performance characteristics from the traditional design that uses the pitch-horn control. For example, servoflap angular deflection not only changes blade aerodynamic coefficients but also leads to servoflap rotor systems where the minimum-power required condition for a flat pitch on the ground does not correspond to zero rotor thrust—a unique design situation not shared by other approaches [6,9,10]. From an engineering point of view, a successful and effective servoflap rotor system hinges upon accurate identification of many design parameters such as the relationships between blade/flap control position, airload distribution, and vibrations induced by a servoflap in both the rotating and the fixed systems [8,11–14]. Though challenging, some of these essential design parameters that affect system performance in different flight conditions can be effectively identified and analyzed through carefully planned instrumentation and utilization of modern signal processing techniques [8–10,13,15,16]. These complexities encountered in servoflap rotor design, however, are rewarded by a number of major performance benefits [9]. Kaman Aerospace Corporation currently manufactures three different types of servoflap based rotors for commercial helicopters.

Servoflap rotor blade torque and power are directly related to aerodynamic characteristics such as drag and lift coefficients, which are determined by the combination of rotor blade angle of attack and servoflap deflection angle. Because the performance of the servoflap rotor system is largely determined by both servoflap control and the relationships between servoflap and rotor blade design parameters in flight, we have expanded on previous studies [15,16] in this paper to further examine servoflap bending and its effects on rotor blade flatwise bending and torsion during four representative flight conditions: hover, transition, minimum-power, and cruising-speed forward flights. This study is important in that bending and torsion affect servoflap deflection angle and rotor blade angle of attack, two critical parameters that determine aerodynamic characteristics of drag and lift coefficients. In addition, because design parameters in the rotating system immediately affect the vibrations induced at the fixed system, any research results that lead to better knowledge regarding how these design parameters are related to the servoflap will consequently provide great assistance to servoflap rotor design. We have used the vibratory data collected from a well-tuned four-bladed helicopter (Fig. 3). The dimension of the main rotor blade is 266 in. long in radius and 23 in. wide chordwise; the servoflap, on the other hand, is only 36 in. long and 8 in. wide. The weights of the rotor blade and the servoflap are around 312 lb (including rotor hub and blade retention weight) and 3 lb, respectively.

Section II of the paper reviews and quantifies the influence of servoflap deflection angle on drag and lift coefficients and rotor blade torque. The input and feedback signals that manipulate the servoflap angle are also described. Section III summarizes multichannel spectral coherence analysis methodolgy [17–19] and the weighted overlapped segment averaging (WOSA) algorithm [18] used in this paper. In Sec. IV, analysis results derived from four different flight conditions are presented. We have analyzed vibratory data of servoflap bending and rotor blade flatwise bending at 17 and 24% of the blade radius and blade torsion at 38% of the blade radius and established the baseline information up to the first eight harmonics of $1/\text{rev}$ frequency. The linear relationships between servoflap bending and rotor blade flatwise bending and torsion are described using magnitude squared coherence and phase delays.

II. Servoflap Rotor Aerodynamics and Control

Although the basic physics, aerodynamics, and fundamental design of servoflap rotor systems and conventional pitch-horn rotor systems remain similar, one major challenge is to accurately determine rotor blade and servoflap pitching moments within an entire operating envelope. Because servoflap pitching moments control servoflap motion and determine control system loads, servoflap size and location are chosen according to the required pitching moments. Kaman has been manufacturing servoflap rotors for more than 50 years; all Kaman servoflap rotors use an external aft flap mounted at 75% of the radius on the trailing edge of each blade (Fig. 1).

Aerodynamic characteristics such as lift coefficient C_L and drag coefficient C_d are critical parameters in servoflap rotor design to generate the maximum main rotor blade pitching moment per degree of servoflap motion for effective blade control in flight. The total

Fig. 3 The servoflap on a composite rotor blade.

blade lift coefficient for a servoflap rotor (without the consideration of compressibility and stall effects [10]) is a primary function of both blade angle of attack α and servoflap angle δ. Flight test data used in the analysis were collected below rotor stall conditions. A simplified lift coefficient equation is given as

$$C_L = C_{L0} + C_{L\alpha}\alpha + C_{L\delta}\delta \tag{1}$$

C_{L0} is the blade lift at zero angle of attack, $C_{L\alpha}$ is the blade lift curve slope, and $C_{L\delta}$ is the servoflap lift curve slope that is unique to servoflap rotor design. One design flexibility of the servoflap rotor reflected in Eq. (1) is that there exists multiple combinations of blade angle of attack α and servoflap angle δ to achieve the same blade lift condition, and such performance flexibility is exclusive to the servoflap rotor.

An analytical expression for the total blade drag coefficient C_d, without considering the effects of compressibility and blade stall, can be simplified as a function of blade angle of attack α and servoflap angle δ, that is,

$$C_d = C_{d0} + C_{d1\alpha}\alpha + C_{d2\alpha}\alpha^2 + C_{d1\delta}\delta + C_{d2\delta}\delta^2 + C_{d1\alpha\delta1}\alpha\delta + C_{d2\alpha\delta1}\alpha^2\delta + C_{d1\alpha\delta2}\alpha\delta^2 + C_{d2\alpha\delta2}\alpha^2\delta^2 \tag{2}$$

It includes drag constant C_{d0}, drag function of blade angles of attack $C_{d1\alpha}\alpha$ and $C_{d2\alpha}\alpha^2$, drag function of servoflap angles $C_{d1\delta}.\delta$ and $C_{d2\delta}.\delta^2$, and blade and servoflap interference drags $C_{d1\alpha\delta1}.\alpha\delta$, $C_{d2\alpha\delta1}.\alpha^2\delta$, $C_{d1\alpha\delta2}.\alpha\delta^2$, and $C_{d2\alpha\delta2}.\alpha^2\delta^2$. Components including servoflap angle δ are unique to servoflap rotors. The complex composition of servoflap blade drag coefficient in Eq. (2) renders the actual design difficult and challenging. Both lift coefficient and drag coefficient affect rotor blade torque and power. For example, the blade element torque dQ is given by

$$dQ = r(dD + \phi dL) = \tfrac{1}{2}\rho\Omega^2 r^3 c(C_d + \phi C_L)dr \tag{3}$$

where ϕdL represents the induced drag resulting from blade element lift dL tilting backward toward the plane of rotation due to inflow angle ϕ. The total torque can be obtained by integrating dQ over the blade radius r.

The servoflap control rod assembly provides the connection between the retention and rotor blade controls; the control linkage is divided into two categories, one for primary control input and the other for feedback control input. As the main rotor blade responds to primary control inputs, it also causes the blade retention assembly to rotate about its longitudinal axis. This rotational movement is picked up by the feedback crank and transmitted to the feedback idler and the idler then changes the moment arm of the retention control level. The control system analysis for servoflap input is given by

$$\delta_{\text{input}} = \delta_0 - \delta_{1s}\sin\psi - \delta_{1c}\cos\psi + K_{\delta\beta}w' + K_{\delta\theta}\theta + K_{\delta\zeta}v' \tag{4}$$

Azimuth coefficients correspond to collective δ_o and cyclic δ_{1s} and δ_{1c} control input. Coefficients $K_{\delta\beta}$, $K_{\delta\theta}$, and $K_{\delta\zeta}$ correspond, respectively, to mechanical feedback couplings from an out-of-plane bending slope w', in-plane bending slope v', and blade feathering displacement–leading edge up from the shaft plane θ. A schematic of the servoflap rotor feedback control system is depicted in Fig. 4. At the current setup, the pilot provides a steady 1/rev control signal to the servoflap rotor during flight while the feedback control crank and idler system introduce higher harmonics control inputs to the system. Although the control signal is currently configured for performance optimization at 1/rev frequency, it is possible to further improve rotor performance with an appropriate feedback control input at harmonics higher than 2/rev frequency. Because of the control input for servoflap is at 1/rev frequency, it is of more interest in this study to examine the linear relationships between servoflap bending and rotor blade bending and torsion at 1/rev. To allow feedback control signals optimized at higher harmonics, additional tests and analyses are currently being conducted by the authors.

III. Multichannel Spectral and Coherence Analysis

The main goal of this study includes 1) identifying vibratory energy concentrations of servoflap bending and rotor blade flatwise bending and torsion at multiple harmonics of 1/rev frequency, and 2) quantifying the linear relationships of these spectral energy concentrations between servoflap bending and rotor blade flatwise bending and torsion. To achieve this goal, multichannel spectral and coherence analysis is used. To illustrate, we consider the spectral density matrix $\Phi(f)$ for an M-channel stationary discrete-time series $[\{x_1(n)\}, \{x_2(n)\}, \ldots \{x_M(n)\}]$,

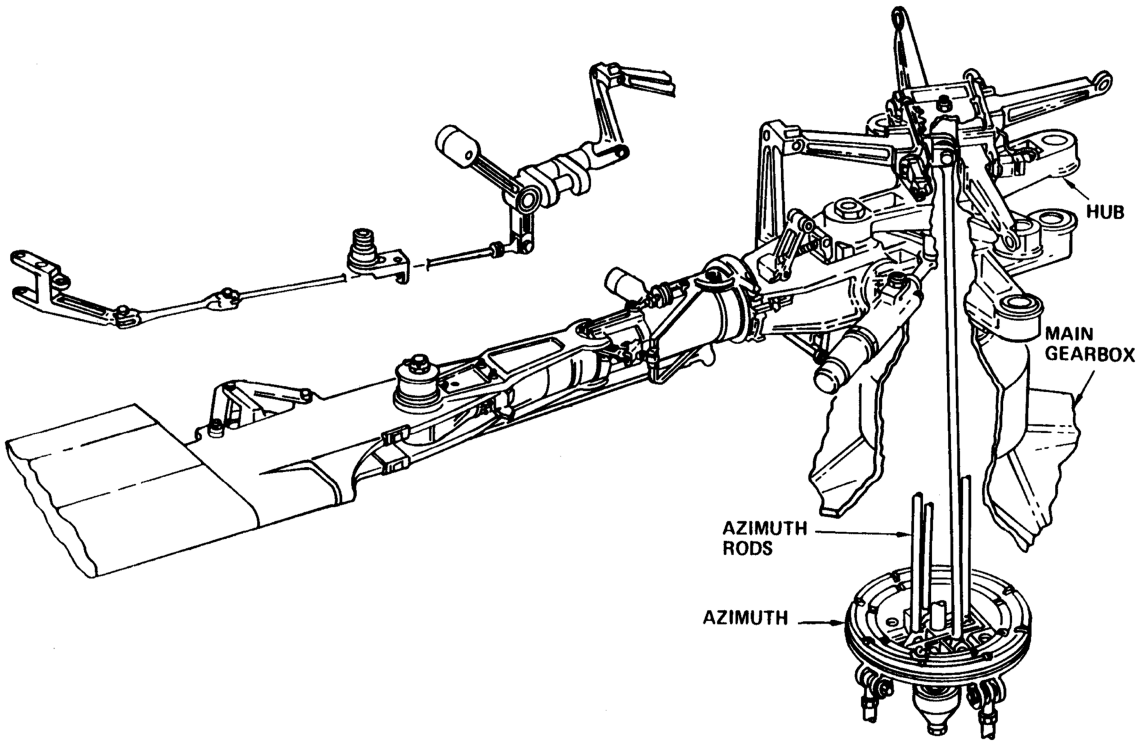

Fig. 4 A schematic of the servoflap rotor control system.

$$\Phi(f) = \begin{bmatrix} S_{11}(f) & S_{12}(f) & \cdots & S_{1M}(f) \\ S_{21}(f) & S_{22}(f) & \cdots & S_{2M}(f) \\ \vdots & \vdots & \ddots & \vdots \\ S_{M1}(f) & S_{M2}(f) & \cdots & S_{MM}(f) \end{bmatrix} \tag{5}$$

The main diagonal terms $\{S_{i,i}(f), i = 1, 2, \ldots, M\}$ in $\Phi(f)$ represent autospectra (or power spectra), which are real valued, positive defined functions representing the energy distribution in the frequency domain. The cross-spectra $\{S_{i,j}(f), i \neq j\}$ off the main diagonal are complex functions containing correlation information between $\{x_i(n)\}$ and $\{x_j(n)\}$. The coherence function [17] is a cross spectrum normalized by the square root of the product of two autospectra and is specified as follows

$$\text{coh}_{i,j}(f) = \frac{S_{i,j}(f)}{\sqrt{S_{i,i}(f)\, S_{j,j}(f)}} \tag{6}$$

A frequency adopted function derived from the coherence is the magnitude squared coherence (MSC), $\text{MSC}(f) = |\text{coh}(f)|^2$. The theoretical value of MSC lies between 0 (indicating $\{x_i(n)\}$ and $\{x_j(n)\}$ uncorrelated) and 1 (complete correlation). The angle of $\text{coh}_{i,j}(f)$ indicates the phase delay between $\{x_j(n)\}$ and $\{x_i(n)\}$ at frequency f. In practice, the MSC value is meaningfully interpreted at frequency f only if $S_{i,i}(f)$, $S_{j,j}(f)$, and $S_{i,j}(f)$ are nonzero.

In the signal processing community, there are many parametric and nonparametric based multichannel spectral analysis algorithms that are successfully developed and reported in the literature [16,18], each having its own merits and limitations. We have chosen the WOSA algorithm [17] in this study to estimate power spectra and coherence functions. The WOSA algorithm has been proved robust, effective, and computationally efficient through the usage of fast Fourier transform. It divides the underlying multichannel time series into many (L) shorter segments of equal length where adjacent segments are overlapped by 50%. Each data segment is multiplied by a tapering function $w(n)$ to provide a smooth transition near both ends of a segment. The Hanning window function [16,18] is chosen for this study. To illustrate, the Fourier transform of the kth weighted segment of $\{x_i(n)\}$ is shown as

$$X_i^k(f) = \frac{1}{N} \sum_{n=0}^{N-1} x_i^k(n) w(n) e^{-j\frac{2\pi f}{N} n} \tag{7}$$

The power spectrum $S_{i,i}(f)$ or cross-spectrum $S_{i,j}(f)$ thus estimated by the WOSA algorithm is obtained by averaging over all available data segments as follows:

$$S_{i,j}(f) = \frac{1}{L} \sum_{k=1}^{L} X_i^k(f) (X_j^k(f))^* \tag{8}$$

where $*$ indicates the complex conjugate.

In addition to spectral energy distribution in the frequency domain, we also developed vibratory energy measures in time domain to quantify average vibratory energy. They are

$$Engy_dc = \frac{1}{L} \sum_{k=1}^{L} \mu_k^2 \tag{9}$$

and

$$Engy_vbr = \frac{1}{L} \sum_{k=1}^{L} \left(\frac{1}{N} \sum_{n=1}^{N} (x^k(n) - \mu_k)^2 \right) \tag{10}$$

where μ_k is the mean value of the kth data segment. *Engy_dc* in Eq. (9) provides a measure of the static portion of servoflap bending and rotor blade bending and torsion vibratory energy. *Engy_vbr* in Eq. (10) provides, on the other hand, an energy index specifically associated with vibratory deformation of servoflap bending and rotor blade bending and torsion by removing the static component (μ_k) in each segment, that is, in statistical term, variance. The total vibratory energy (*Engy_total*) is the sum of *Engy_dc* and *Engy_vbr*. Because of the large dynamical ranges of vibratory data, these three energy indices are more conveniently represented in decibels (dB). It is worth mentioning that in spectral estimation using Eq. (8) the mean value of each segment (μ_k) is removed from the data.

IV. Helicopter Flight Data Analysis

As explained previously in Eqs. (1) and (2), the servoflap rotor angle δ and rotor blade angle of attack α both affect rotor blade aerodynamic characteristics in the lift coefficient C_L and the drag coefficient C_d. Therefore, it is of great interest to servoflap rotor designers to be able to identify the relationships between servoflap and key design parameters of the rotating system. In an effort to answer that call, we chose to study vibratory energy of servoflap midspan vertical bending (*Flap*) at multiple harmonics of 1/rev frequency and to examine its effects on main rotor blade flatwise bending at 17% ($B17f$) and 24% ($B24f$) of the blade radius, respectively, and blade torsion at 38% ($B38t$) of the blade radius. $B17f$ and $B24f$ were chosen, in particular, because of their close proximity (7% of blade radius apart), and their flight behaviors are expected to be similar. However, any minor differences observed from close proximity can often leave important clues to help in understanding of how the influence of servoflap bending is physically distributed along the rotor blade radial direction. We have expanded previous studies [15,16] by including four representative helicopter flights: hover (*Hover*), transition (*Trans*)—forward flight between 40 to 50 kt, minimum-power ($Adv17$)—forward flight at 70-kt and cruising-speed ($Adv27$) forward flight. Vibratory data used in this paper were collected from Kaman SH-2G servoflap rotor [8,9,11] with 298 rpm. Helicopter vibratory data of *Flap*, $B17f$, $B24f$, and $B38t$ are calculated at multiple harmonics of 1/rev frequency (i.e., $298/60 \approx 5$ Hz); the linear relationships of *Flap* vs $B17f$, *Flap* vs $B24f$, and *Flap* vs $B38t$ are quantified using MSC and phase delays. Flight data used in this study were measured using strain gauges and collected with a sampling rate of 500 Hz. The power spectrum and the cross spectrum were estimated using the WOSA algorithm with 500 samples in each segment and adjacent segments were overlapped by 250 samples.

A. Vibratory Energy Distribution at Harmonics of 1/rev Frequency

Figure 5 displays vibratory data plots of servoflap bending during hover, transition, minimum-power and cruising-speed forward flights in the left column and power spectral estimates in a frequency span from 0 to 50 Hz in the right column. In Fig. 5a, servoflap bending energy in hover (*Hover*) is most prominent at harmonics of 1/rev, 3/rev, and 5/rev and exhibits a spectral energy concentration at 5/rev frequency more than other flights. When compared against power spectra during transition (*Trans*) and forward flights ($Adv17$ and $Adv27$), we notice that servoflap bending energy at 1/rev frequency is increased by 7.2 dB (5.25 times), 6.49 dB (4.46 times), and 8.58 dB (7.21 times), respectively. Similar observations are also noted at higher harmonics, except at 3/rev frequency during *Trans* (Fig. 5b) where spectral energy is considerably reduced by 14.75 dB (or down by 96.65%). During transition flight, servoflap bending has experienced a drastic change in spectral energy distribution: an insignificantly small energy at 3/rev frequency and relatively high energy at 4/rev frequency. The dynamic ranges of servoflap bending are roughly $(-400 \rightarrow 200)$ in *Hover*, $(-860 \rightarrow 275)$ in *Trans*, $(-950 \rightarrow 250)$ in $Adv17$, and $(-860 \rightarrow 650)$ in $Adv27$. During *Hover*, servoflap exhibits the least vibratory variation. Energy indices defined in Eqs. (9) and (10) are summarized in Table 1.

In Table 1 we note that servoflap bending has the least energy during hover flight. The relatively higher values of *Engy_dc* during *Trans* and $Adv17$ flights are consistent with the data plots shown in Figs. 5b and 5c. One can also find in Table 1 that, although servoflap bending exhibits more vibratory energy (*Engy_vbr*) during cruising-speed forward flight ($Adv27$) than minimum-power forward flight ($Adv17$) by 2.39 dB (1.73 times), static deformation energy (*Engy_dc*) during $Adv17$ is 7.61 dB (5.77 times) more than that of $Adv27$ flight. The numbers in Table 1 are expressed in decibels and

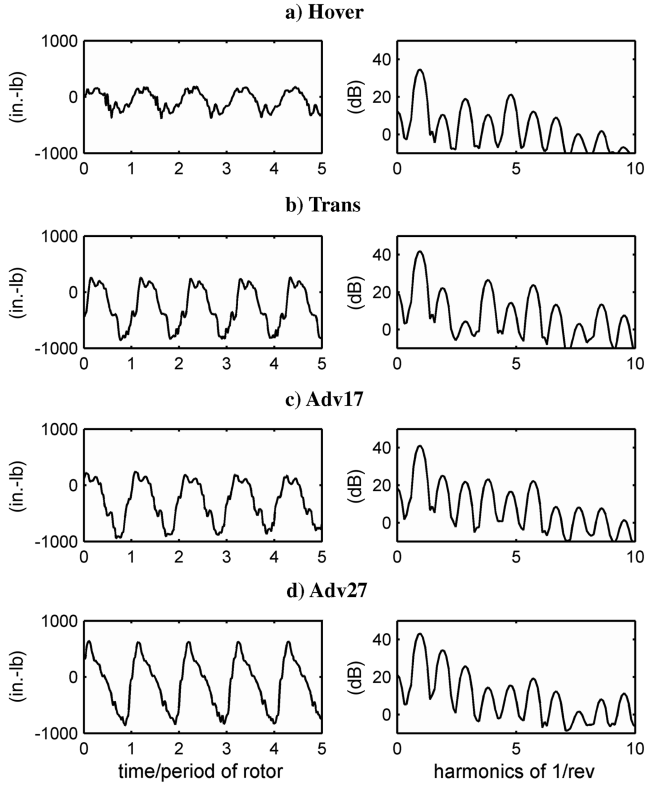

Fig. 5 Servoflap midspan vertical bending: *Flap* (left column) and power spectra (right column) in different flights.

the relationship of *Engy_dc* (dB), *Engy_vbr* (dB) and *Engy_total* (dB) is related by the following:

$$10^{Engy_dc(\mathrm{dB})/10} + 10^{Engy_vbr(\mathrm{dB})/10} = 10^{Engy_total(\mathrm{dB})/10} \tag{11}$$

Spectral energies of the first eight harmonics of servoflap bending are summarized in Table 2; spectral patterns of servoflap bending (*Flap*) during *Trans* and $Adv17$ flights are generally similar, except for the lower energy at 3/rev (4.35 dB) and higher at 4/rev (26.58 dB) frequencies during *Trans* flight. In Table 2, we can see that when forward flight shifts from minimum power ($Adv17$) to cruising speed ($Adv27$), the spectral energy of *Flap* also encounters a major increase at 2/rev ($24.78 \rightarrow 34$ dB) and reduction at 4/rev ($23.26 \rightarrow$ 14.48 dB) frequencies, that is, increased to 8.36 times at 2/rev and reduced to 13.2% at 4/rev frequencies, respectively.

Rotor blade flatwise bending at 17 and 24% ($B17f$ and $B24f$) of the blade radius and power spectra are displayed in Figs. 6 and 7, respectively. Because of the close proximity of measurement locations and the exact characteristics of measurement, flatwise bending, vibratory data, and power spectra derived from $B17f$ and $B24f$ are similar to each other. However, the differences between them can provide valuable information regarding incremental changes of rotor blade performance along the feathering axis.

A noticeable difference in vibratory data plots in Figs. 6 and 7 is that rotor blade flatwise bending $B24f$ shows more static bending during all four flight conditions than that of $B17f$. For example, the dynamic range of $B24f$ during *Hover* is ($2.277\mathrm{E}+4 \rightarrow 3.114\mathrm{E}+4$) in Fig. 7a while the dynamic range for the same flight condition is ($1.468\mathrm{E}+4 \rightarrow 2.363\mathrm{E}+4$) in Fig. 6a. During the $Adv27$ flight, the dynamic ranges of $B24f$ and $B17f$ are ($1.935\mathrm{E}+4 \rightarrow 3.093\mathrm{E}+4$) in Fig. 7d and ($1.07\mathrm{E}+4 \rightarrow 2.161\mathrm{E}+4$) in Fig. 6d, respectively. Note that they are different in mean value μ_k; dynamic ranges of $B17f$ and $B24f$, on the other hand, are very close. We can observe from the results in Table 1 that *Engy_dc* values of $B24f$ are 3 dB larger than those of $B17f$ while *Engy_vbr* values remain similar.

Spectral energies of the first eight harmonics of 1/rev frequency in Figs. 6 and 7 are listed in Table 3. It is noticed in Table 3 that the power spectra of $B17f$ and $B24f$ are very similar to each other in four examined flight conditions—spectral energies at 1/rev and 2/rev frequencies generally increase steadily from *Hover* to *Trans* to $Adv17$ to $Adv27$. One evident exception, however, is that the spectral energies of $B17f$ (Fig. 6d) and $B24f$ (Fig. 7d) at 4/rev frequency during $Adv27$ are 13.5 and 14.49 dB smaller than *Hover*. A similar observation is also observed at 5/rev frequency, 4.22 dB in $B17f$ and 3.92 dB in $B24f$. Both $B17f$ and $B24f$ show more spectral energies during cruising speed ($Adv27$) than minimum-power forward flight ($Adv17$) at 1, 2, 3, 5, and 7/rev harmonics, but this observation is reversed at spectral energies at 4, 6, and 8/rev harmonics. This pattern is also found in the power spectral peaks of servoflap bending in Table 2. This pattern similarity is linked to the feedback couplings described in servoflap control input Eq. (4). As a result of an appropriate servoflap 1/rev control input, reduction of servoflap bending at higher harmonics of 4, 6, and 8/rev was achieved and thus the reduction of blade flatwise bending at the same harmonics.

Vibratory data of rotor blade torsion at 38% of the blade radius ($B38t$) and power spectra are displayed in Fig. 8. Power spectral peaks of the first eight harmonics of 1/rev frequency are summarized in Table 4. Compared against vibratory data of $B17f$ and $B24f$, blade flatwise torsion $B38t$ has a dynamic range of variation that is much different in magnitude (Table 1). We know from design experiences that spectral energies at multiple harmonics of the rotating speed in Fig. 8 are caused primarily by a servoflap aerodynamic pitching moment that moves main rotor blades and generates blade torsion moments with all harmonics. During *Hover*, power spectral energies are more pronounced at 1 and 5/rev frequencies (Fig. 8a) whereas spectral peaks are more evident at 1 and 6/rev frequencies during *Trans* (Fig. 8b) and $Adv17$ (Fig. 7c). The spectral energy of $B38t$ at 1/rev frequency during *Hover* (38.71 dB) only slightly increases during *Trans*, $Adv17$, and $Adv27$ but the increment is much bigger at 2/rev frequency, for example, 16.33 dB (43 times larger) increment from *Hover* to $Adv27$. An interesting pattern of power spectra we have observed in all three rotating system parameters ($B17f$, $B24f$, and $B38t$) is that during cruising-speed flight ($Adv27$) power spectral energies at 1, 2, 3, 5, and 7/rev frequencies are larger than those of minimum-power forward flight ($Adv17$) but the situation is reversed at 4, 6, and 8/rev frequencies, a result of the servoflap feedback couplings.

Table 2 Power spectral peaks of servoflap bending at harmonics of 1/rev frequency (dB)

	Flap							
No./rev	1/rev	2/rev	3/rev	4/rev	5/rev	6/rev	7/rev	8/rev
Hover	34.66	10.35	19.1	10.64	21.13	12.32	9.14	−0.14
Trans	41.86	21.86	4.35	26.58	14.21	23.89	13.4	3.13
$Adv17$	41.15	24.78	22.03	23.26	16.47	22.38	8.61	8.17
$Adv27$	43.24	34.0	25.88	14.48	15.31	19.37	12.43	1.57

Table 1 Three energy indices during four flights: *Engy_dc*, *Engy_vbr*, and *Engy_total* (dB)

	Flap			$B17f$			$B24f$			$B38t$		
Flight cond.	*dc*	*vbr*	*total*	*dc*	*vbr*	*total*	*dc*	*vbr*	*total*	*dc*	*vbr*	*total*
Hover	36.53	44.20	44.89	85.49	64.66	85.53	88.56	64.19	88.57	48.91	53.27	54.62
Trans	48.65	51.25	53.15	84.66	71.13	84.85	88.23	70.63	88.31	55.44	58.21	60.05
$Adv17$	49.23	50.62	52.99	84.61	67.83	84.70	88.22	67.73	88.26	55.86	56.89	59.41
$Adv27$	41.62	53.01	53.32	84.59	68.96	84.71	88.29	69.42	88.34	50.35	56.40	57.36

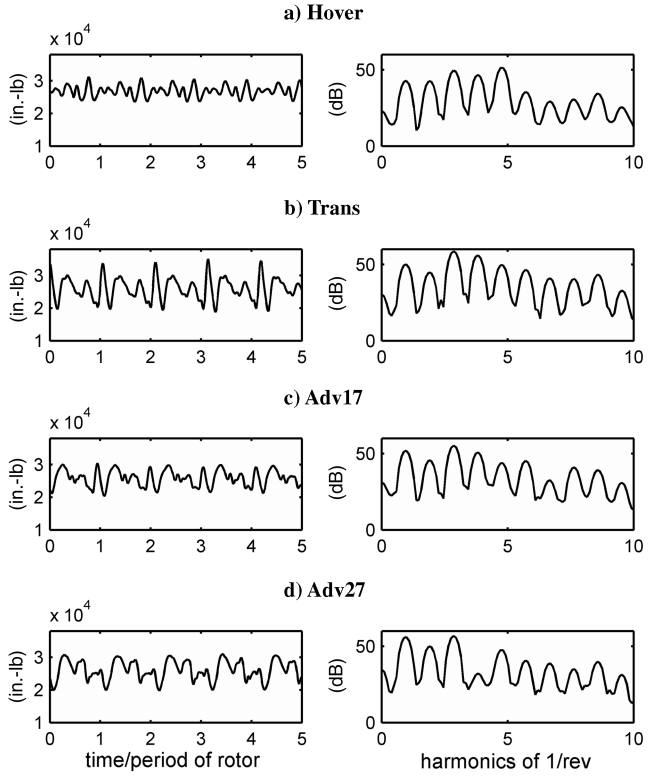

Fig. 6 Rotor blade flatwise bending at 17% of rotor blade radius: $B17f$ (left column) and power spectra (right column) in different flights.

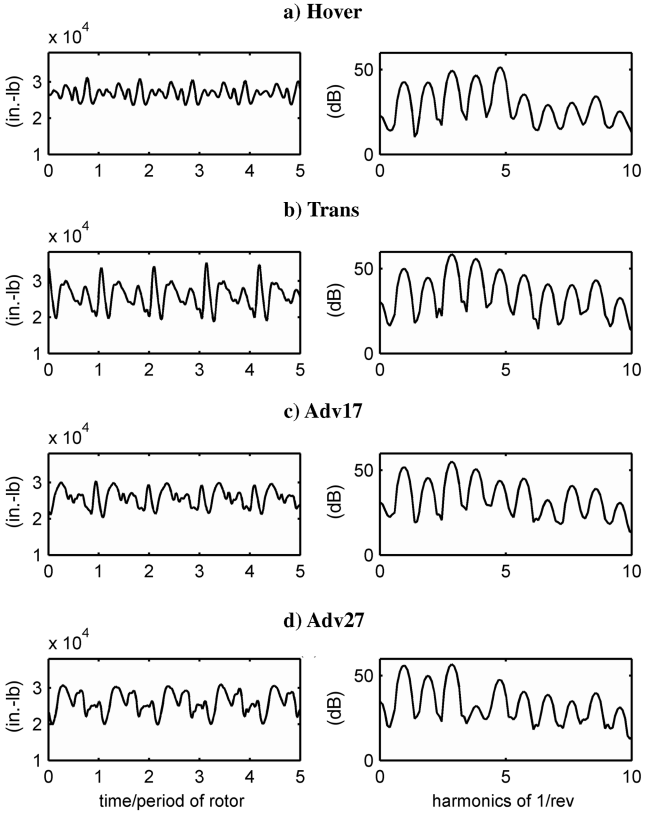

Fig. 7 Rotor blade flatwise bending at 24% of rotor blade radius: $B24f$ (left column) and power spectra (right column) in different flights.

To provide a different perspective, the spectral energies of the first eight harmonics of 1/rev frequency summarized in Tables 2–4 are delineated by the flight condition in Fig. 9. $B17f$ and $B24f$ display identical spectral energy patterns in all four flight conditions and both show a significant bending reduction of 24 dB at 4/rev frequency in forward-cruising flight (Fig. 9d) and a 12 dB reduction at 7/rev frequency in minimum-power forward flight (Fig. 9c). Blade torsion $B38t$ also exhibits a similar spectral pattern to that of $B17f$ and $B24f$, except in *Trans* flight where the power spectrum shows a small increment at 6/rev frequency (Fig. 9b). Another interesting observation is that in $Adv17$ (Fig. 9c) all vibratory measurements, $Flap$, $B17f$, $B24f$, and $B38t$, show a local minimum at 5/rev frequency; however, in $Adv27$ (Fig. 9d) that local minimum appears at 4/rev frequency.

B. Coherence Function and Phase Delay

The linear relationships between servoflap bending and rotating system design parameters, $Flap$-$B17f$, $Flap$-$B24f$, and $Flap$-$B38t$, were examined using cross-spectra and coherence functions. Figures 10–13 show the cross-spectra ($|S_{i,j}(f)|^2$), MSC and phase coherence functions during four different flights. During *Hover* flight (Fig. 10), the cross-spectral peaks are mutual energies between *Flap* and rotor blade design parameters $B17f$, $B24f$, and $B38t$ at harmonics of 1/rev frequency. However, the magnitude of these mutual energies in cross spectra does not indicate the significance of correlation. The correlation significance MSC must be verified using Eq. (6) by including the power spectra of individual design parameters in Fig. 5; phase coherence is also estimated when a significant MSC is scored.

Results in $Flap$-$B17f$ (Fig. 10a) and $Flap$-$B24f$ (Fig. 10b) are similar due to the physical proximity of $B17f$ and $B24f$. The correlations of spectral energies between *Flap* and $B17f$ (Fig. 10a) show significant MSC values larger than 0.9 and near 1 at the first six harmonics; a smaller MSC value of 0.8 is observed at 8/rev harmonics in both Figs. 10a and 10b. It should be noted that although the power spectrum at 2/rev frequency of *Flap* during *Hover* (Fig. 5a) is weak at 10.35 dB (Table 2), it is closely correlated with the much stronger spectral energies at 2/rev frequency in both $B17f$ (Fig. 6a) and $B24f$ (Fig. 7a). MSC values of the first eight harmonics during all tested flight conditions are summarized in Table 5.

In Fig. 10c, the coherence ($Flap$-$B38t$) shows strong correlations (with MSC values near 1) at most harmonics (under 6/rev), with an exception of a weaker correlation (MSC = 0.759) at 2/rev frequency. The phase coherence functions are displayed in the bottom row of Fig. 10. They provide phase delay estimates at multiple harmonics of 1/rev frequency. During *Hover*, there is a positive phase delay of 36.67 deg at 1/rev frequency in $Flap$-$B17f$ (Fig. 10a), which indicates that the servoflap bending (*Flap*) leads $B17f$ by 36.67 deg (≈20.51 ms with 298 rpm) after the 1/rev servoflap control input is initiated. The phase lead at 1/rev frequency is reduced to 28.31 deg (≈15.83 ms) in $Flap$-$B24f$ (Fig. 10b). The small difference of 8.36 deg (≈4.68 ms) between $Flap$-$17f$ and $Flap$-$B24f$ reflects the fact that the strain gauge placement of $B24f$ is only 7% (blade radius) closer to the servoflap than $B17f$. In other words, the *Flap* control input at 1/rev frequency affected $B24f$ first and then $B17f$ after a short delay. It is conceivable that if more strain gauges are placed in incremental locations to measure rotor blade

Table 3 Power spectral peaks of blade flatwise bending at harmonics of 1/rev frequency (dB)

				$B17f$				
No./rev	1/rev	2/rev	3/rev	4/rev	5/rev	6/rev	7/rev	8/rev
Hover	42.89	41.69	49.87	47.24	51.88	36.23	30	31.98
Trans	49.01	43.4	59.14	56.3	50.22	47.57	42.54	42.17
*Adv*17	50.36	44	55.66	51.17	44	46.23	34.22	42.23
*Adv*27	54.36	48.25	57.03	33.76	47.66	42	39.96	35.56
				$B24f$				
No./rev	1/rev	2/rev	3/rev	4/rev	5/rev	6/rev	7/rev	8/rev
Hover	42.77	42.2	49.48	46.69	51.32	35.54	29.37	30.41
Trans	50.06	44.4	58.62	55.92	49.5	46.49	41.04	40.39
*Adv*17	51.87	45.18	55.21	50.78	43.63	45.28	32.5	40.87
*Adv*27	56.04	49.58	56.77	32.2	47.4	40.69	38.83	34.96

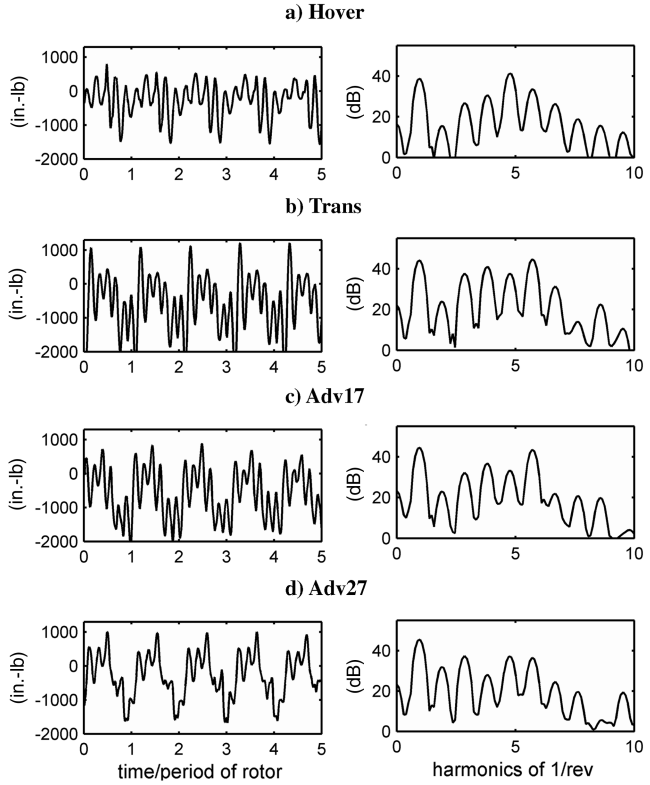

Fig. 8 Rotor blade torsion at 38% of rotor blade radius: *B38t* (left column) and power spectra (right column) in different flights.

flatwise bending, a detailed profile regarding the phase delay along blade radius can be more precisely documented. There is a positive phase delay of 17.13 deg (≈9.58 ms) at 1/rev frequency in *Flap-B38t* (Fig. 10c); this is consistent with the sensor location of *B38t*, 14% (of the blade radius) closer to servoflap than *B24f*.

With regard to the phase delays at harmonics higher than 1/rev frequency, it should be noted first that the underlying servoflap rotor studied in this paper was designed by adjusting mechanical feedback coupling coefficients $K_{\delta\beta}$, $K_{\delta\theta}$, and $K_{\delta\zeta}$ to provide an optimal 1/rev servoflap control in different flight conditions. To adjust coefficients $K_{\delta\beta}$, $K_{\delta\theta}$, and $K_{\delta\zeta}$ for the servoflap control at higher harmonics, power spectral energies and coherence functions are useful indexes. Repeated adjustments of coefficients for that purpose must be made and coherence values measured to provide the baseline data for qualitative and quantitative analysis. A servoflap control input aimed at higher than 1/rev is currently under investigation by the authors. In Fig. 10, the phase delays in *Flap-17f* and *Flap-B24f* of 2/rev frequency are both at about 29.3 deg (≈16.39 ms). We also observe from the phase plots in Figs. 10a and 10b that the phase difference between *Flap-17f* and *Flap-B24f* remains almost the same at all harmonics higher than 1/rev frequency. On the other hand, the phase plot of *Flap-B38t* (Fig. 10c) changes rapidly from 1 to 3/rev. For ease of comparison, the first two harmonics during the four flight conditions are listed in Table 6.

Cross spectra, MSC, and phase delay estimates during transition flight (*Trans*) are displayed in Fig. 11. At 1/rev frequency, there are strong mutual energies and significant MSC values in *Flap-B17f*,

Table 4 Power spectral peaks of blade flatwise torsion at harmonics of 1/rev frequency (dB)

	B38t							
No./rev	1/rev	2/rev	3/rev	4/rev	5/rev	6/rev	7/rev	8/rev
Hover	38.71	15.27	26.81	30.68	41.18	33.64	26.42	18.76
Trans	44.07	23.53	37.77	41.02	37.4	44.69	31.36	13.88
*Adv*17	44.46	22.66	32.19	36.78	33.0	43.5	21.91	20.7
*Adv*27	45.44	31.6	37.34	28.02	36.95	36.51	24.58	19.56

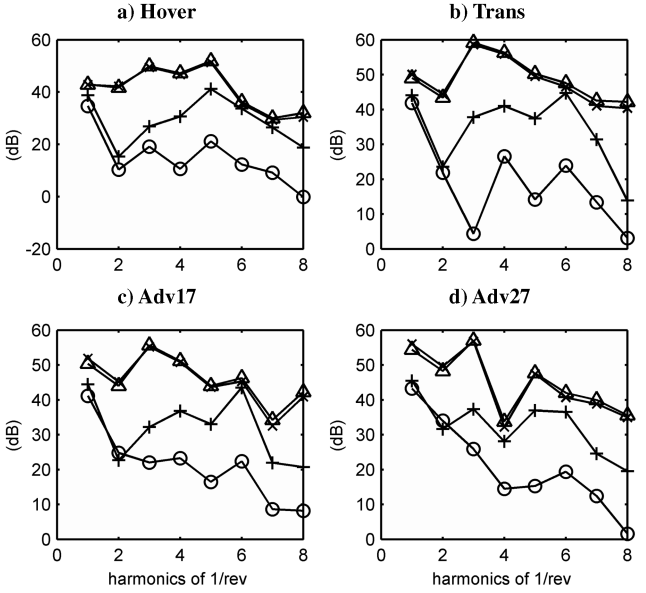

Fig. 9 Spectral energies of *Flap* (○), *B17f* (△), *B24f* (×), and *B38t* (+) in four different flights.

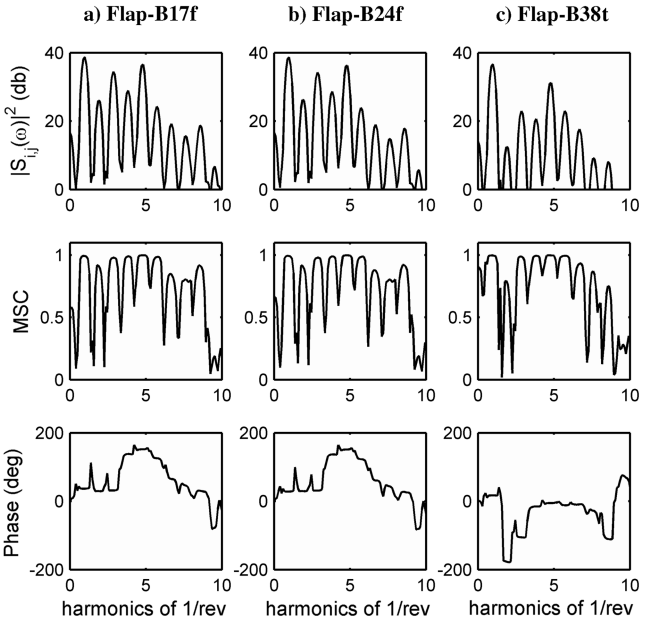

Fig. 10 Cross spectra, MSC, and phase delays during hover.

Flap-B24f, and *Flap-B38t* with phase delays of 23.4, 16.02, and 32.11 deg, respectively. There remains a minor phase difference (7.4 deg) between *B17f* and *B24f*. However, unlike *Hover* flight, the phase delay in *Flap-B38t* (Fig. 11c) at 1/rev frequency is larger than that of *Flap-B24f* (Fig. 11b). This is largely due to the high degree of nonlinear aerodynamics and interactions between the servoflap and rotor blade during transition flight that prevents a simple explanation based on the physical locations. At 2/rev frequency there remains a strong correlation with high MSC values in *Flap-B17f*, *Flap-B24f*, and *Flap-B38t* (Fig. 11); the phase delays are −165.5, −170, and 4.53 deg, respectively. Note that there is a phase wrapping of 2π(360 deg) in our phase measurements. One visible observation in Fig. 11 is that a very low MSC value near 0.56 (weak correlation) appears at 3/rev frequency in *Flap-B17f*, *Flap-B24f*, and *Flap-B38t*, a result of a small spectral energy at 3/rev frequency of *Flap* in *Trans* (Fig. 5b).

Figures 12 and 13 display the cross spectra, MSC, and phase delay estimates in minimum-power (*Adv*17) and cruising-speed (*Adv*27)

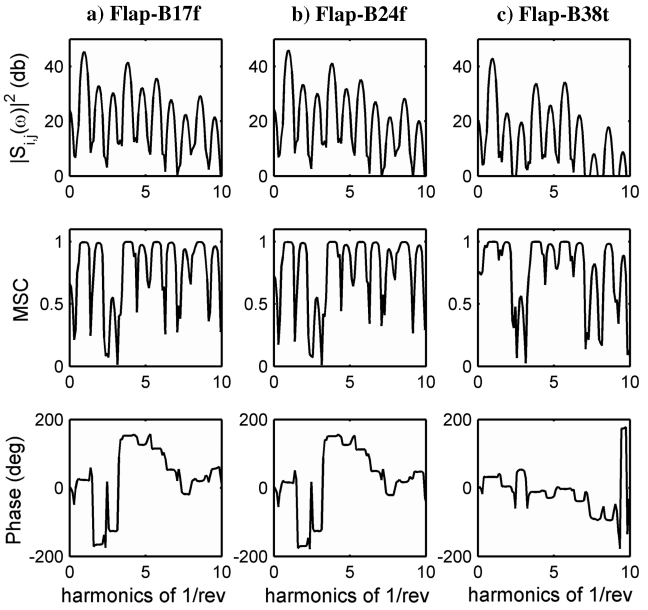

Fig. 11 Cross spectra, MSC, and phase delays during transient flight.

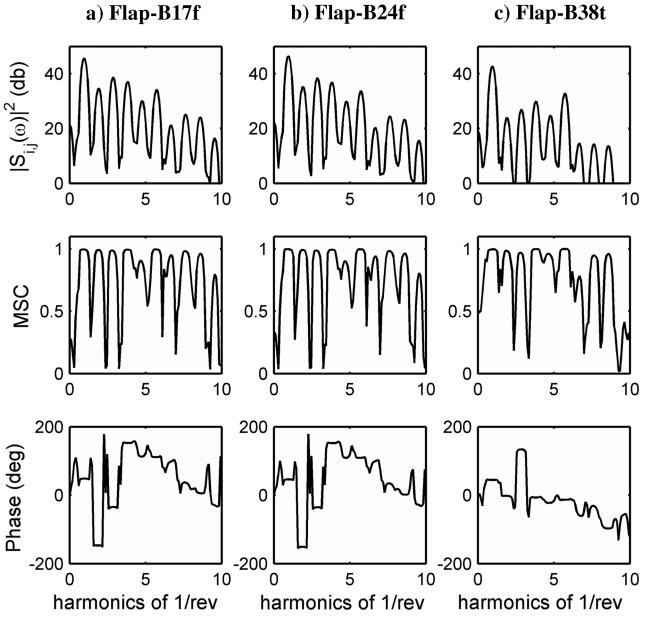

Fig. 12 Cross spectra, MSC, and phase delays during minimum-power forward flight.

forward flights. In $Adv17$ flight, the linear relationships of $Flap\text{-}B17f$, $Flap\text{-}B24f$, and $Flap\text{-}B38t$ are highly significant at 1/rev frequency with MSC values near 1; corresponding phase delays are 48.67, 46.37, and 44.8 deg, respectively (Table 6). In $Adv27$ flight, the same relationships are maintained at 1/rev frequency; phase delays in $Flap\text{-}B17f$, $Flap\text{-}B24f$, and $Flap\text{-}B38t$ are 80.03, 79.94, and 55.08 deg, respectively. These observations in Figs. 12 and 13 show that spectral energies (at 1/rev frequency) of servoflap bending and rotor flatwise bending and torsion are linearly correlated and phase delays too correspond to the physical locations of gauge placements.

Although the linear correlations at 2/rev frequency are also significant in Figs. 12 and 13, phase delays, on the other hand, no longer bear the correlation in physical locations of sensor placement as observed at 1/rev frequency. For example, phase delays are −146.6, −150.8, and −2.13 deg, respectively, in Fig. 12 during $Adv17$; phase delays are 179.7, 176.9, and 15.84 deg, respectively, in Fig. 13 during $Adv27$. In the cross spectra of $Flap\text{-}B38t$, there is a

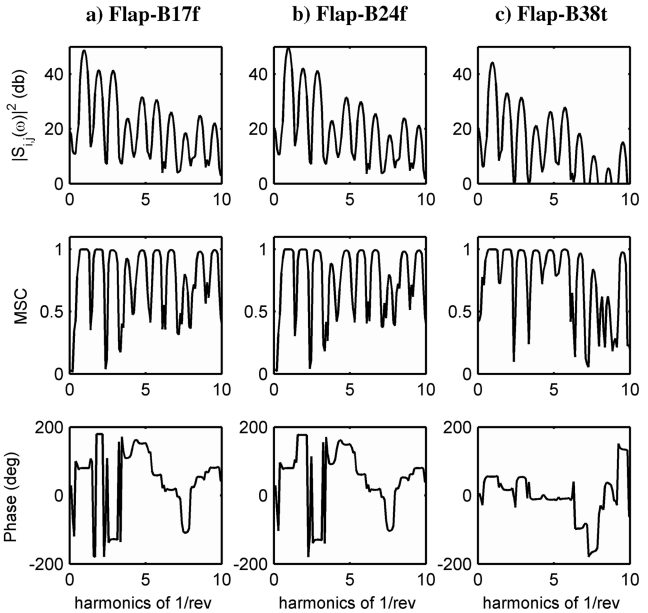

Fig. 13 Cross spectra, MSC, and phase delays in cruising-speed forward flight.

slightly larger cross-spectral energy at 4/rev frequency during $Adv17$ (Fig. 12c) than that of $Adv27$ (Fig. 13c), but the situation is reversed at 5/rev frequency. This observation coincides well with power spectral analysis results that spectral energy at 4/rev frequency is significantly larger in *Flap* (Figs. 5c and 5d) and $B38t$ (Figs. 8c and 8d) during $Adv17$ while the spectral energy at 5/rev frequency in $B38t$ during $Adv27$ is 3.95 dB larger than $Adv17$ (Table 4). By comparing MSC plots in Figs. 12c and 13c, we can observe that, regardless of the difference in cross-spectra magnitudes, MSC values at 4 and 5/rev frequencies are near 1 in $Flap\text{-}B38t$ during both $Adv17$ and $Adv27$ (Table 5). Further study and more test data are required in the future.

V. Conclusions

Servoflap rotor design presents an interesting task for engineers. The additional degree of freedom in servoflap rotors makes the overall design different and unique, for example, to accurately determine rotor blade and servoflap pitching moments within an entire operating envelope. Because of the inherent complexity of the servoflap rotor, the qualitative behavior is to be derived and confirmed through test flights and quantitative analysis. In this paper, we have examined servoflap rotor design parameters under four

Table 5 MSC values at harmonics of 1/rev frequency

				Flap-B17f				
No./rev	1/rev	2/rev	3/rev	4/rev	5/rev	6/rev	7/rev	8/rev
Hover	0.992	0.896	0.979	0.99	0.998	0.984	0.844	0.803
Trans	0.99	0.99	0.555	0.99	0.97	0.99	0.99	0.92
*Adv*17	0.996	0.991	0.986	0.995	0.88	0.996	0.954	0.982
*Adv*27	0.999	0.998	0.992	0.915	0.991	0.992	0.994	0.769
				Flap-B24f				
No./rev	1/rev	2/rev	3/rev	4/rev	5/rev	6/rev	7/rev	8/rev
Hover	0.993	0.893	0.979	0.99	0.998	0.985	0.875	0.802
Trans	0.997	0.99	0.555	0.99	0.971	0.998	0.995	0.919
*Adv*17	0.998	0.992	0.986	0.995	0.978	0.997	0.945	0.982
*Adv*27	0.999	0.999	0.992	0.875	0.99	0.992	0.993	0.768
				Flap-B38t				
No./rev	1/rev	2/rev	3/rev	4/rev	5/rev	6/rev	7/rev	8/rev
Hover	0.997	0.759	0.9817	0.994	0.998	0.995	0.932	0.847
Trans	0.999	0.995	0.564	0.999	0.978	0.999	0.991	0.823
*Adv*17	0.997	0.983	0.969	0.999	0.943	0.999	0.785	0.948
*Adv*27	0.999	0.999	0.994	0.991	0.993	0.998	0.966	0.817

Table 6 Phase delays between servoflap and rotor blade parameters (deg)

Flight cond.	1/rev			2/rev		
	*Flap-B*17f	*Flap-B*24f	*Flap-B*38t	*Flap-B*17f	*Flap-B*24f	*Flap-B*38t
Hover	36.67 deg	28.31 deg	17.13 deg	29.31 deg	29.37 deg	−177.8 deg
Trans	23.4 deg	16.02 deg	32.11 deg	−165.6 deg	−170 deg	4.53 deg
*Adv*17	48.67 deg	46.37 deg	44.8 deg	−146.6 deg	−150.8 deg	−2.13 deg
*Adv*27	80.03 deg	79.94 deg	55.08 deg	179.7 deg	176.9 deg	15.84 deg

representative helicopter flight conditions using multichannel spectral and coherence analysis. The results have provided the baseline data of power spectral energies measured from servoflap bending, rotor blade flatwise bending, and torsion, including the linear relationship between servoflap bending and rotor blade design parameters, at multiple harmonics of the rotating speed. As a result, we have derived a quantity of useful information that can be used to facilitate servoflap rotor design.

1) Servoflap bending in all four test flights exhibits significant linear relationships with the examined rotating system parameters ($B17f$, $B24f$, and $B38t$). Coherence analysis has confirmed via the MSC measure the significance of correlation at the first six harmonics of 1/rev frequency in all flight conditions, with an exception at 3/rev frequency during transition flight.

2) In hover, the phase coherence provides an accurate estimate of phase delays at 1/rev frequency between servoflap and rotating system parameters such as a phase delay of 36.67 deg (≈20.51 ms) between *Flap* and $B17f$, 28.31 deg (≈15.83 ms) between *Flap* and $B24f$, and a phase delay of 17.13 deg (≈9.58 ms) between *Flap* and $B38t$. These numbers are consistent with the servoflap rotor design tuned at 1/rev frequency control.

3) During hover flight, rotor blade flatwise bending and torsion exhibit the highest spectral energy at 5/rev frequency; servoflap bending shows the highest energy at 1/rev frequency, followed by the second highest peak at 5/rev frequency. Servoflap bending and blade torsion both see a substantial energy sink at 2 and 4/rev harmonics. Blade flatwise bending measurements show a gradual, small spectral energy increment from 1 up to 5/rev frequency and then a quick drop after 6/rev frequency.

4) During transition flight, servoflap bending exhibits a spectral energy distribution different from hover flight, a minimum spectral energy at 3/rev frequency and high energy at 4/rev frequency. Contrary to servoflap bending, both rotor blade flatwise bending measurements show the highest energy concentration at 3/rev frequency.

5) When the forward flight condition was switched from minimum power to cruising speed, the spectral energies of servoflap bending, rotor flatwise bending, and rotor torsion at 1, 2, 3, 5, and 7/rev frequencies increased whereas spectral energies at 4, 6, and 8/rev frequencies decreased, most pronounced at 4/rev frequency. This is largely due to the fact that, although the mechanical feedback couplings in the test helicopter were adjusted at 1/rev frequency control to optimize the performance, these flight tests were conducted by a four-blade helicopter and the spectral energy reduction at $4x$/rev vibrations was fed back to servoflap input.

6) The phase relationships found between servoflap bending and blade design parameters at higher harmonics (≥ 2) of 1/rev frequency have to be considered by taking into account the feedback from rotor blades. For example, the phase delays can be altered through the feedback coefficients and provide useful indexes in adjusting the servoflap control to achieve the desired performance. The involved complexity prevents a simple physical interpretation as in the case of 1/rev frequency. Continuing efforts to include 2/rev input for the servoflap control are currently being conducted by the authors.

References

[1] Johnson, W., *Helicopter Theory*, Dover, New York, 1980.

[2] Leishman, J. G., *Principles of Helicopter Aerodynamics*, 2nd ed., Cambridge Univ. Press, New York, 2006.

[3] Lemnios, A. Z., and Jones, R., "The Servo-Flap—An Advanced Rotor Control System," *American Helicopter Society Design Specialists' Meeting on Vertical Lift Aircraft Design*, American Helicopter Society, Alexandria, VA, Jan. 1990.

[4] Toulmay, F., Kloppel, V., Lorin, F., Enenkl, B., and Gaffiero, J., "Active Blade Flaps—The Needs and Current Capabilities," *57th American Helicopter Society Annual Forum*, American Helicopter Society, Alexandria, VA, May 2001.

[5] Wei, F. S., "Design of an Integrated Servo-Flap Main Rotor," *American Helicopter Society 59th Annual Forum*, American Helicopter Society, Alexandria, VA, June 2003.

[6] Wei, F. S., "Advanced Servo-Flap Rotor Using Variable Blade Index Angle Control," *38th AIAA/ASME/ ASCE/AHS/ASC Structures, Structural Dynamics, & Materials Conference*, AIAA, Reston, VA, April 1997.

[7] Straub, F. K., and Merkley, D. J., "Design of a Servo-Flap Rotor for Reduced Control Loads," *Smart Materials & Structures*, Vol. 5, 1996, pp. 68–75. doi:10.1088/0964-1726/5/1/008

[8] Tischler, M. B., and Tomashofski, C. A., "Flight Test Identification of SH-2G Flapped-Rotor Helicopter Flight Mechanics Models," *Journal of American Helicopter Society*, Vol. 47, No. 1, Jan. 2002, pp. 18–32.

[9] Wei, F. S., and Gallagher, F., "Servo-Flap Rotor Performance Flight Testing and Data Identification," *American Helicopter Society 57th Annual Forum*, American Helicopter Society, Alexandria, VA, May 2001.

[10] Wei, F. S., and Ning, T., "Performance Analysis for the Servo-flap Rotor," *2nd International Basic Research Conference on Rotorcraft Technology*, American Helicopter Society, Nanjing, China, 7–9 Nov. 2005, pp. 424–433.

[11] Wei, F. S., and Jones, R., "Dynamic Tuning of the SH-2F Composite Main Rotor Blade," *American Helicopter Society 43rd Annual Forum*, American Helicopter Society, Alexandria, VA, May 1987.

[12] Wei, F. S., Basile, J. P., and Jones, R., "Vibration Reduction on Servo Flap Controlled Rotor Using HHC," *AHS National Specialists Meeting on Rotorcraft Dynamics*, American Helicopter Society, Alexandria, VA, Nov. 1989.

[13] Gallagher, F., and Wei, F. S., "Flight Testing Kaman Aerospace Corporation's Composite Main Rotor Blade," *American Helicopter Society 56th Annual Forum*, American Helicopter Society, Alexandria, VA, May 2000.

[14] Rocconella, B., and Wei, F. S., "Wind Tunnel Model Testing of the Improved K-MAX Servo-Flap Blade Section," *American Helicopter Society 57th Annual Forum*, American Helicopter Society, Alexandria, VA, May 2001.

[15] Ning, T., and Wei, F. S., "Multichannel Coherence Analysis of Helicopter Vibrations," *IEEE 6th International Conference on Signal Processing*, IEEE, Piscataway, NJ, 26–30 Aug. 2002, Vol. 2, pp. 1774–1777.

[16] Ning, T., Wei, F. S., and Suen, A. J., "Servo-Flap Rotor Design Parameters Identification via Spectral Analysis of Flight Data," *46th AIAA Aerospace Sciences Meeting and Exhibit*, AIAA, Reston, VA, 7–10 Jan. 2008.

[17] Carter, G. C. (ed.), *Coherence and Time Delay Estimation*, Institute of Electrical Electronics Engineers, Inc., New York, 1993.

[18] Carter, G. C., Knapp, C. H., and Nuttall, A. H., "Estimation of the Magnitude-Squared Coherence Function Via Overlapped Fast Fourier Transform Processing," *IEEE Transactions on Audio and Electroacoustics*, Vol. 21, No. 4, 1973, pp. 337–344. doi:10.1109/TAU.1973.1162496

[19] Cadzow, J. A., and Solomon, O. M., Jr., "Linear Modeling and the Coherence Function," *IEEE Transactions on Acoustics, Speech, and Signal Processing*, Vol. 35, No. 1, Jan. 1987, pp. 19–28. doi:10.1109/TASSP.1987.1165022

J. Cooper
Associate Editor